Journal of Hydrology 414–415 (2012) 86–98

Contents lists available at SciVerse ScienceDirect

Journal of Hydrology

journal homepage: www.elsevier.com/locate/jhydrol

A remote sensing approach for estimating the location and rate of urban irrigation in semi-arid climates

Tyler D. Johnson *, Kenneth Belitz

US Geological Survey, California Water Science Center, San Diego, CA, USA

ARTICLE INFO

Article history:
Received 25 October 2010
Received in revised form 7 October 2011
Accepted 13 October 2011
Available online 25 October 2011
This manuscript was handled by Philippe Baveye, Editor-in-Chief, with the assistance of Magdeline Laba, Associate Editor

Keywords:
Urban irrigation
Remote sensing
Evapotranspiration
Landsat
NDVI
Endmembers

SUMMARY

Urban irrigation is an important component of the hydrologic cycle in many areas of the arid and semi-arid western United States. This paper describes a new approach that uses readily available datasets to estimate the location and rate of urban irrigation. The approach provides a repeatable methodology at 1/3 km^2 resolution across a large urbanized area (500 km^2). For this study, Landsat Thematic Mapper satellite imagery, air photos, climatic records, and a land-use map were used to: (1) identify the fraction of irrigated landscaping in urban areas, and (2) estimate the monthly rate of irrigation being applied to those areas. The area chosen for this study was the San Fernando Valley in Southern California.

Identifying irrigated areas involved the use of 29 satellite images, air photos, and a land-use map. The fraction of a pixel that consists of irrigated landscaping (F_{irr}) was estimated using a linear-mixture model of two land-cover endmembers (selected pixels within a satellite image that represent a targeted land-cover). The two endmembers were impervious and fully-irrigated landscaping. In the San Fernando Valley, we used airport buildings, runways, and pavement to represent the impervious endmember; golf courses and parks were used to represent the fully irrigated endmember. The average F_{irr} using all 29 satellite scenes was 44%. F_{irr} calculated from hand-digitizing using air photos for 13 randomly selected single-family-residential neighborhoods showed similar results (42%).

Estimating the rate of irrigation required identification of a third endmember: areas that consisted of urban vegetation but were not irrigated. This "nonirrigated" endmember was used to compute a Normalized Difference Vegetation Index (NDVI) surplus, defined as the difference between the NDVI signals of the irrigated and nonirrigated endmembers. The NDVI signals from irrigated areas remains relatively constant throughout the year, whereas the signal from nonirrigated areas rises and falls seasonally due to precipitation. The areas between airport runways were chosen to represent the nonirrigated endmember. Water-delivery records from 65 spatially-distributed single-family neighborhoods, consisting of nearly 1800 homes, were correlated with the NDVI surplus. The results show a strong exponential correlation ($r^2 = 0.94$).

In the absence of water-delivery records, which can be difficult to obtain, a surrogate was identified: the landscape evapotranspiration rate (ET_L). ET_L was used to scale NDVI surplus (which is dimensionless) to irrigation rates using an exponential scaling function. The monthly irrigation rates calculated from satellite and climatic data compared well with irrigation rates calculated from actual water-delivery data using a paired Wilcoxan signed-rank test ($p = 0.0063$).

Identification of F_{irr} at the pixel scale, along with identification of the irrigation rate for a fully-irrigated pixel, allows for mapping of urban irrigation over large areas. Maps showing the location and rate of monthly irrigation for the San Fernando study area were computed for January and August 1997.

Published by Elsevier B.V.

1. Introduction

Urban irrigation is an important component of the hydrologic cycle in many areas of the arid and semi-arid western United States. Urban irrigation can influence the groundwater hydrologic cycle by increasing the amount of water available to infiltration through return flow (Grimmond et al., 1986), and can influence the surface water hydrologic cycle by affecting runoff rates from rainfall events (Sample and Heaney, 2006). By understanding how urban irrigation affects the hydrologic cycle water-management agencies can: (a) be better prepared for alterations in the water supply, whether due to climatic, engineered, or catastrophic reasons, (b) model and track changes in water chemistry, and (c) test future consumptive use scenarios (Hurd et al., 1999; Vörösmarty et al., 2000; Jacobs et al., 2001; Alcamo et al., 2008).

* Corresponding author. Tel.: +1 619 225 6100; fax: +1 619 225 6101.
E-mail address: tyjohns@usgs.gov (T.D. Johnson).

0022-1694/$ - see front matter Published by Elsevier B.V.
doi:10.1016/j.jhydrol.2011.10.016

The volume of urban irrigation being applied to the landscape can be significant, exceeding natural rainfall in certain arid areas (California Department of Water Resources (CDWR) 1975). Among the urban land-use classes that contain irrigated landscaping, the largest volume of water is typically used in residential areas (Grimmond and Oke, 1986; CDWR, 1994; San Diego County Water Authority (SDCWA), 2001; City of Los Angeles Department of Water Power LADWP, 2001; Western Research Advocates (WRA), 2003). Studies have shown that more than 50% of the water used in a typical household per year is used outside the home (Grimmond and Oke, 1986; Mayer et al., 1999). For the residential areas within the city of Los Angeles for example, this equates to nearly 225 million cubic meters of water being used for irrigation per year, potentially influencing the urban hydrologic cycle (LADWP, 2000, 2001; Southern California Area Governments (SCAG), 2005). Therefore, a cost effective and repeatable technique for estimating urban irrigation at local and regional scales is needed.

A number of methods for estimating urban irrigation have been previously used including the use of data loggers, the minimum-month method, and energy balance formulas (Mayer et al., 1999; Gleick et al., 2003). However, many of these or similar methods can be cost and time prohibitive, difficult to implement on a regional scale, and/or inaccurate at the local scale.

An alternative method of estimating urban irrigation is through the use of satellite remote sensing. Remote sensing has been shown to be an effective method for quantifying vegetation cover/density, and for estimating evapotranspiration (ET), both of which have been shown to relate to residential and commercial irrigation (Mayer et al., 1999; Keith et al., 2002). The Normalized Difference Vegetation Index (NDVI) (Rouse et al., 1974) has been used for many years to detect actively photosynthesizing plants (Myneni et al., 1995; Jensen, 2000). NDVI has also been used to estimate evaporation and transpiration values (Courault et al., 2005). Szilagyi and Parlange (1999) correlated NDVI with evaporation for five watersheds across the United States. Keith et al. (2002) noted correlations between evaporation, salinity, and water usage with variations in NDVI. Groeneveld et al. (2007) was able to predict evapotranspiration of groundwater using NDVI and other data. These investigators showed that a satellite-derived vegetation index was a useful tool for monitoring water usage at the regional and sub-watershed scales. In addition, researchers have used a combination of remote sensing (incorporating the thermal band) and the energy balance equation in estimating ET such as the Surface Energy Balance Algorithm for Land (SEBAL) (Bastiaanssen et al., 1998, 2005) and the Mapping Evapotranspiration at High Resolution with Internalized Calibration (METRIC) algorithm (Allen et al., 2005, 2007).

The objective of this paper is to describe a new approach that uses readily available datasets to estimate the location and rate of urban irrigation in arid and semi-arid climates. Our approach is unique in that is uses household water-delivery records to calibrate a derivative of NDVI with climatic data. The approach provides a repeatable methodology at a 1/3 km^2 scale across a large urbanized area (500 km^2). For this study, satellite imagery, air photos, climatic records, and a land-use map were used to: (1) identify irrigated urban areas, and (2) estimate the monthly rate of irrigation being applied to those areas.

The study area chosen to test and apply this new approach is the San Fernando Valley in Southern California (Fig. 1). This area was chosen because of the availability of water use records acquired during previous work (Johnson, 2005). Geographically, the Valley is bounded by the San Gabriel and Santa Susana Mountains to the north, the Santa Monica Mountains to the south, the Verdugo Mountains to the east, and the Simi Hills to the west (Fig. 1). The San Fernando Valley has a Mediterranean climate with rainfall occurring primarily in the late fall and winter months resulting in cyclical greening and browning of nonirrigated urban vegetation. Annual average rainfall is approximately 452 mm (National Oceanic Atmospheric Administration, 2002) The greater San Fernando Valley had a population of approximately 1.7 million in 2008 (US Census, 2008).

2. Datasets and development

2.1. Landsat imagery

There are many remote sensing platforms that could potentially be used for this study. However, Landsat Thematic Mapper 5 (Landsat) has a number of benefits including long-term temporal coverage, a large spatial extent per scene, moderate pixel size (30 m) and ease of acquisition. The Landsat satellites pass over the same location every 16 days, providing nearly continuous coverage since 1984. One satellite image covers more than 30,000 km^2 (this encompasses the entire San Fernando Valley). Numerous studies have shown the 30-m resolution of Landsat to be adequate for mapping vegetation (Chen and Cihlar, 1996; Ma et al., 2001; Homer et al., 2004). Landsat images are archived and freely downloadable, allowing retrospective studies to be performed. Two Landsat spectral bands were specifically designed to aid in the quantification of vegetation characteristics (Jensen, 2000). Healthy plants absorb the red band of light, mostly due to chlorophyll, and reflect the near-infrared band, mostly due to cell composition (Myneni et al., 1995). These two bands are used to calculate the Normalized Difference Vegetation Index (NDVI) (Rouse et al., 1974).

Twenty-nine Landsat Thematic Mapper 5 satellite images (Path/Row 41/36, dated 10/1996–3/1999) were acquired from the US Geological Survey (USGS) Earth Resources Observation Systems Data Center, preprocessed for terrain and geospatial correction to minimize spatial distortion and error. (Data available for download at http://landsat.usgs.gov.) Images with excessive cloud cover or other atmospheric conditions that compromised the NDVI signal over the study area were removed based upon visual inspection, but cloud cover was generally below 20% for the entire image. Digital numbers for the red and the near-infrared spectral bands were converted to radiances using the gain and offset values provided with each image, adjusted for exoatmospheric solar irradiance. This helps minimize reflectance differences that occur when comparing multiple image dates due to differences in sun angle and Earth–Sun distance. These conversions are explained by Chander et al. (2009). The NDVI value for each pixel ($NDVI_p$) was calculated using the following equation (Rouse et al., 1974), for all 29 scenes:

$$\mathrm{NDVI}_p = \frac{NIR_p - Red_p}{NIR_p + Red_p} \quad (1)$$

where NIR_p is the near-infrared radiance recorded in band 4 (wavelengths from 0.76 to 0.90 μm), and Red_p is the visible red radiance recorded in band 3 (wavelengths from 0.63 to 0.69 μm).

The unitless NDVI values range from −1 to 1 with healthy plants typically having values greater than 0.5 and non-vegetation classes, such as water, having 0 or negative NDVI values.

2.2. Climatic data

The monthly potential evapotranspiration [ET_o (t)] for the San Fernando Valley was acquired using the nearest California Irrigation Management Information System (CIMIS) station located in Glendale, CA. (Data available for download at http://wwwcimis.water.ca.gov.) The city of Glendale is in the neighboring San Gabriel Valley and has a similar climate to the San Fernando Valley, occupying the same ET zone (CDWR, 2010). Potential ET values represent the amount of water alfalfa can evapotranspire for a given period of time.

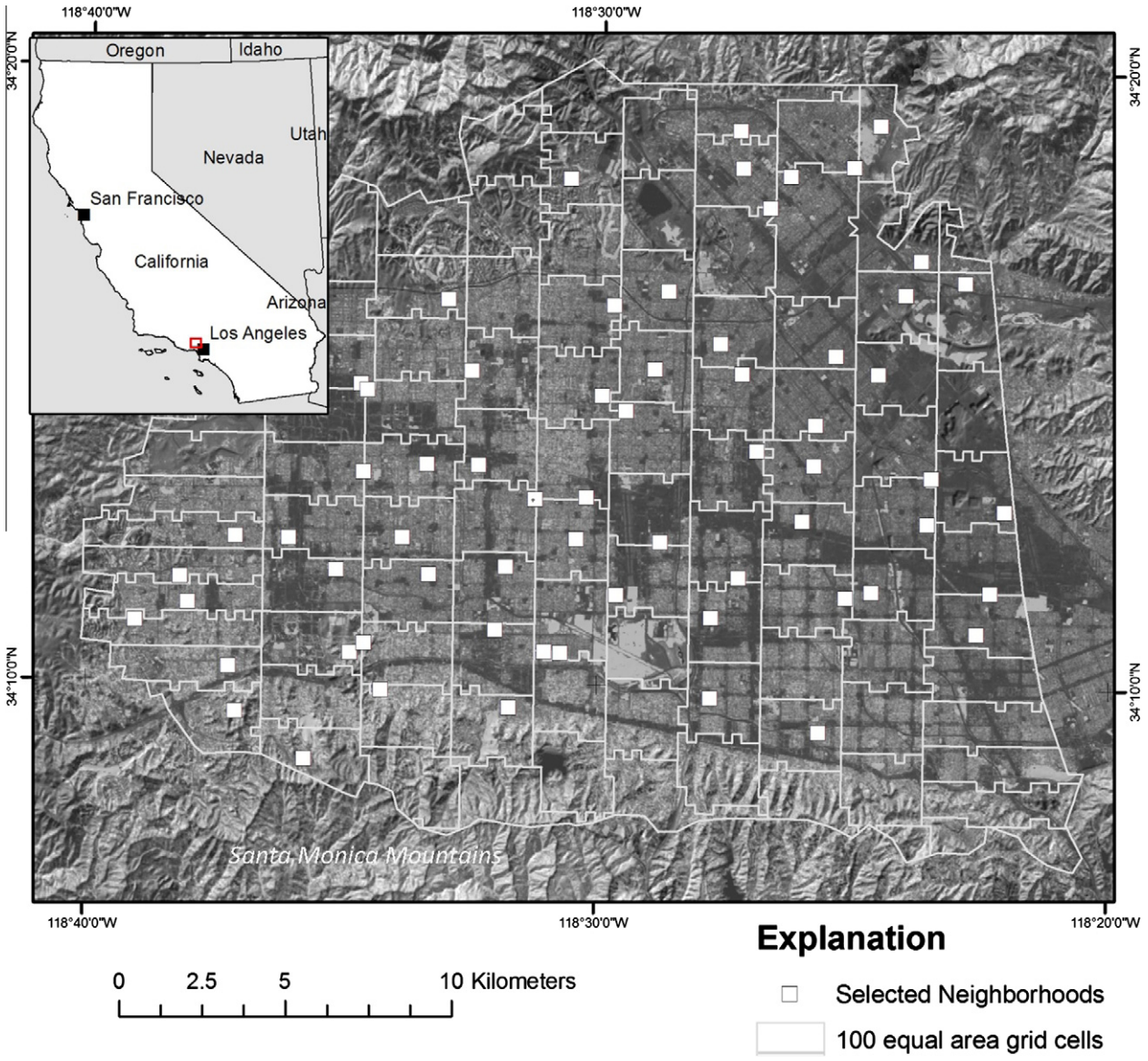

Fig. 1. NDVI image (10/5/1996) of the San Fernando Valley, CA. Lighter areas are more vegetated, darker areas are less vegetated. Study area was divided into 100 equal area cells. Sixty-five randomly selected neighborhoods shown as white squares.

A landscape evapotranspiration rate [$ET_L(t)$] was calculated by multiplying $ET_o(t)$ by a landscape coefficient (K_L). The landscape coefficient is similar to a crop coefficient except that it incorporates additional factors besides the crop type. These factors can be the amount of shading the vegetation receives, localized wind speeds, the density of the plant growth, total canopy cover, and the type of plant itself, among other factors (CDWR, 2000). Typically, urban landscapes consist of a variety of species with a variety of microclimates, but, in general, turf grasses, trees and bushes dominate, based upon site visits and air photo inspection. Turf grasses use between 60% and 80% of the potential ET (CDWR, 1994; 2000). Also, many typical residential plants have either a "medium" or "high" water-use rating, with 0.60 defining the upper range of the medium category and 0.70 defining the lower range of the high boundary (CDWR, 2000). Based upon these factors, we used a landscape coefficient of 0.65 for this study when computing $ET_L(t)$.

2.3. Land-use and land-cover data

The geospatial boundaries of the 65 neighborhoods were hand digitized on the screen using color aerial imagery (1 m resolution, dated 2005) obtained from the National Agricultural Imagery Program (NAIP). (Data available for download at http://datagateway.nrcs.usda.gov.) The boundaries included half the distance across the surrounding streets because streets make up a component of the urban landscape and would not have been sampled otherwise. It was important to have accurate boundaries because these boundaries determined which pixels would later be selected from the satellite image. If the center of a pixel fell within a delineated neighborhood, it was selected as belonging to that neighborhood.

A land-use dataset was acquired from the Southern California Area Governments (SCAG, 2005) and used to classify and identify areas of the San Fernando Valley where urban irrigation could occur. This land-use map consisted of digitized polygons that grouped land-use classes together. The top five land-use classes (Table 1) make up 75% of the total land area within the study area. All 65 neighborhoods were within the "High-Density Single-Family Residential" (single-family) class. According to SCAG, this land-use class contains single family detached units with a density >2 units/acre. Two additional land-use classes: "Low-Rise Apartments, Condominiums, and Townhouses" (multi-family) and "Modern/Older

Table 1
Top 10 land-use classes (by area) of the San Fernando Valley. *Source*: SCAG 2005.

Land use code	Class	Area m^2	Percent of total	Description	Contains irrigated landscaping
1111	Residential	251,480,846	48.7	High-density single family residential	Yes
3100	Vacant	66,694,103	12.9	Vacant undifferentiated	No
1123	Residential	28,640,391	5.6	Low-rise apartments, condominiums, and townhouses	Yes
1311	Industrial	20,719,653	4.0	Manufacturing, assembly, and industrial services	No
1223/1224	Commercial	18,529,704	3.6	Modern/older strip development	Yes
1112	Residential	14,439,253	2.8	Low-density single family residential	Yes
1413	Transportation	10,875,486	2.1	Freeways and major roads	Yes
1437	Transportation	8553,801	1.7	Improved flood waterways and structures	No
1810	Open space and rec	7428,928	1.4	Golf courses	Yes
1821	Open space and rec	6700,388	1.3	Developed local parks and recreation	Yes

Strip Development" (strip-malls) (SCAG, 2005) also contained irrigated landscaping (based upon visual inspection using NAIP and other high resolution aerial photographs). Two other land use classes: "Vacant Undifferentiated" and "Manufacturing, Assembly, and Industrial Services" were mostly nonirrigated, and therefore not considered in the analysis.

For the purposes of ground truthing, a 20% sample of each land-use class was hand-digitized to determine typical percentages of land-cover. Thirteen neighborhoods from the single-family land-use class (approximately 364 homes), seventeen neighborhoods from the multi-family class, and seventeen strip-malls were digitized at 1:500 scale using high resolution air photos (0.3048 m resolution, dated 2008)) from the Los Angeles Region Imagery Acquisition Consortium (LARIAC) (data available for download at http://planning.lacounty.gov/LARIAC/). In addition to LARIAC, other ancillary imagery was used to help identify vegetation. These included a false-color infrared dataset (1 m resolution, dated 2002) from the USGS National Digital Orthophoto Program (NDOP) (data available for download at http://seamless.usgs.gov/), and a black/white dataset (1 m resolution, dated 1994) from the USGS National Aerial Photography Program (NAPP) (data available for download at http://earthexplorer.usgs.gov).

Two land-cover categories were identified and digitized: (1) impervious hardscape (consisting of rooftops, driveways, sidewalks, streets, etc.), and (2) irrigated landscaping (defined as areas under or potentially under the influence of irrigation). A third land-cover was identified in the single-family class: (3) water (consisting mostly of swimming pools). This method results in the footprint of the landscaped areas being mapped, excluding tree canopies and vegetation overgrowth. Typical landscaping included trees, bushes, and lawns. The land-cover percentages within each land-use class were averaged. See Fig. 2 for an example of hand-digitization of one of the 13 single-family neighborhoods.

Two additional estimates of irrigated landscaping were examined: a local dataset from the Los Angeles County Department of Public Works (LACDPW, 2006), and a national dataset from the USGS called the National Land Cover Dataset (NLCD) (USGS, 2003). Both datasets reported percentage impervious. The LACDPW dataset is a polygon- based dataset that assigned a single percentage impervious value for each land-use class. The NLCD dataset is pixel based. Imperviousness within a targeted land-use class was calculated by taking the average of all the pixels within each class. Milesi et al. (2005) has show that impervious surface area is inversely correlated to turf grass area. Therefore, the percentage pervious was calculated for both datasets by subtracting the imperviousness number from 100%. These datasets were used to compare the reported values of imperviousness/perviousness with our hand-mapped and remotely-sensed values of impervious hardscape/irrigated landscaping.

2.4. Water delivery data

Water delivery data were obtained from the LADPW from a total of 1795 homes within 65 neighborhoods. The randomized and spatially distributed sampling design is described in Johnson (2005). The average neighborhood size was 24,828 m^2 containing 8–55 homes each with an average of 28 homes per neighborhood. Fig. 1 shows the San Fernando Valley divided into equal area grid cells from which the 65 neighborhoods were selected. One neighborhood was selected per cell to avoid spatial bias.

The water delivery data were provided in 2-month billing cycles for the period October 1996 through April 1999. The data were subsequently converted into monthly water delivery rates and averaged for each neighborhood. Water meter readings that contained less than three homes were considered partial readings and not included in the averaging. All neighborhoods were then averaged together to compute an average monthly water delivery rate for the "composite neighborhood." The composite neighborhood is the term used to indicate that the value is an average of all 65 neighborhoods. In addition to water delivery data, NDVI values were also averaged and assigned to the composite neighborhood.

2.5. Identifying NDVI spectral endmembers

Any area being sampled by a Landsat satellite can be considered a linear mixture of spectral "endmembers" (Adams et al., 1995; Roberts et al., 1998). A spectral endmember is one of a number of selected "pure" components of a particular area being mapped. For example, an urban environment may consist of three spectral endmembers of vegetation, impervious, and bare soil (Ridd, 1995), or vegetation, impervious/bare soil, and shade (Lu and Weng, 2004). By identifying the endmembers within a targeted land-use class, each pixel within a satellite scene can be linearly "unmixed" into its respective percentages for each component.

NDVI, which uses bands 3 and 4, has been used to identify urban endmembers of vegetated and non-vegetated (Qi et al., 2000; Song, 2005). Therefore, three NDVI spectral endmembers were identified within the San Fernando Valley: irrigated landscaping, nonirrigated landscaping, and impervious. Two of the endmembers (irrigated landscaping, impervious) were used for mapping the location of irrigated landscaping. Two of the endmembers (irrigated landscaping and nonirrigated landscaping) were used for computing the irrigation rate. Each endmember consisted entirely of its targeted land-cover. For the irrigated-landscaping endmember, eight golf courses/parks were delineated. For the impervious endmember, three local airports consisting of buildings, parking lots, and runways were delineated. The nonirrigated-landscaping endmember was identified by delineating the inter-runway grass areas at three local airports. A fourth endmember (water) was also identified. This endmember was used in validating the methodology but was not used in the final model. Seven local lakes and reservoirs were delineated for the water-body endmember.

Delineation of the endmember target areas was performed onscreen by hand, using reregistered NAIP, LARIAC, NDOP, and NAPP aerial imagery. Google, and Virtual Earth imagery was also used (various acquisition dates and resolutions) as an additional resource for delineating endmembers. The NAIP dataset from

Fig. 2. Example of hand-digitized neighborhood showing three land-covers: impervious hardscape (purple and beige), water (blue), and landscaped vegetation (green). (Rooftops are shown for visualization, but were considered part of the impervious hardscape land-cover.) (For interpretation of the references to color in this figure legend, the reader is referred to the web version of this article.)

1994 was used primarily to ensure that target endmembers existed at the time of the satellite images. The resulting polygons were buffered inward by 15-m (one-half the width of a 30-m pixel) to ensure all pixels representing the endmembers were 100% within the original boundary. The NDVI pixel values for each endmember were extracted from the satellite scenes using the polygons that delineated each endmember. The NDVI pixel values were then averaged together to create one NDVI value per endmember per scene.

3. Methodology

This section is separated into two parts, to address the two goals of this study: (1) estimating the amount and location of irrigated landscaping within urbanized areas, and (2) estimating the rate of irrigation being applied to those areas.

3.1. Estimating the location of irrigated landscaping

The remote sensing technique we used to map the location and fraction of irrigated landscaping within the San Fernando Valley incorporates a two-endmember linear mixture model using NDVI endmembers. The two-endmember model is expressed as:

$$\mathrm{NDVI}_{2end}(t) = (F_{irr} * \mathrm{NDVI}_{irr}(t)) + ((1 - F_{irr}) * \mathrm{NDVI}_{impv}(t)) \quad (2)$$

where $\mathrm{NDVI}_{2end}(t)$ = the NDVI value for a single-family residential neighborhood, computed monthly, F_{irr} = fraction classified as irrigated landscaping, $\mathrm{NDVI}_{irr}(t)$ = NDVI for irrigated-landscape endmember, computed monthly. $\mathrm{NDVI}_{impv}(t)$ = NDVI for the impervious endmember, computed monthly.

Application of Eq. (2) requires an estimate of the fraction of the two endmembers for a given area (the 65 neighborhoods), and the observed NDVI values for the same two endmembers (Fig. 3).

Eq. (2) was rewritten to solve for $F_{irr}(t)$, thus allowing for estimation of F_{irr} in terms of observed NDVI values:

$$F_{irr}(t) = \frac{\mathrm{NDVI}_{2end}(t) - \mathrm{NDVI}_{impv}(t)}{\mathrm{NDVI}_{irr}(t) - \mathrm{NDVI}_{impv}(t)} \quad (3)$$

Eq. (3) can be computed at the pixel level, or at the neighborhood level. At the neighborhood level, $F_{irr}(t)$ is an average of the pixels within that neighborhood. $F_{irr}(t)$ will vary each month because the NDVI signal inputs also vary each month. For the purposes of evaluation, an average value of F_{irr} for the composite neighborhood using all 29 satellite scenes was calculated (Fig. 3). This is expressed as $\overline{F_{irr}}$:

$$\overline{F_{irr}} = \frac{1}{n}\sum_{i=0}^{n} F_{irr}(t) \quad (4)$$

where $\overline{F_{irr}}$ = average fraction of irrigated landscaping for the composite neighborhood, n = number of satellite scenes.

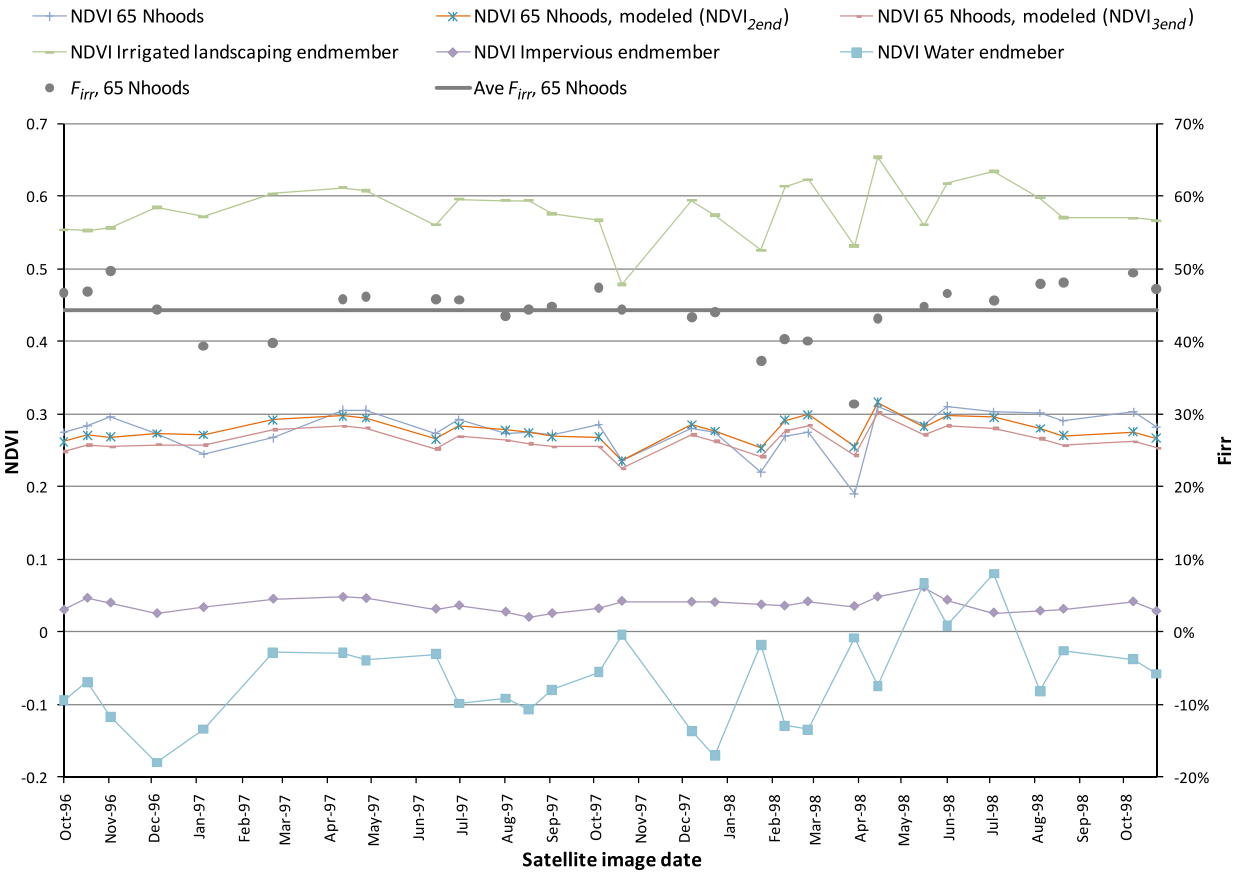

Fig. 3. NDVI values for selected endmembers (Irrigated, Impervious, Water) and 65 single-family residential neighborhoods (65 Nhoods) computed for 29 Landsat satellite scenes. Also shown are the modeled NDVI values for the 65 neighborhoods using a 3-endmember mixture model ($NDVI_{3end}$) and a 2-endmember mixture model ($NDVI_{2end}$). On the secondary axis are the calculated fractions of irrigated landscaping [$F_{irr}(t)$] for the 65 neighborhoods. The average F_{irr} ($\overline{F_{irr}}$) is shown as a solid line.

3.2. Estimating landscape irrigation rates

Water delivered to a neighborhood can be divided into two components: water used to irrigate landscaping, and water used for other purposes. Those other purposes could include water used inside the home, or outside for things such as washing cars. Water used for irrigation will contribute to the NDVI signal, whereas water used for other purposes will not. Our goal was to use the NDVI signal for estimating the water used for irrigation.

3.2.1. Relating NDVI and water delivery

In urbanized areas without irrigation in the San Fernando Valley, there is a cyclical pattern in NDVI resulting from a greening of vegetation in the fall and winter, followed by a browning of the vegetation in the summer (Fig. 4). In contrast, irrigated landscaping, supported by water delivery, maintains a relatively constant value of NDVI throughout the year (Fig. 4). In this paper "NDVI surplus" [NDVI_$S(t)$] is defined as the difference between the NDVI observed in the fully irrigated endmember and the NDVI observed in the nonirrigated endmember:

$$\text{NDVI\_}S(t) = \text{NDVI}_{irr}(t) - \text{NDVI}_{nonirr}(t) \quad (5)$$

where NDVI_$S(t)$ = NDVI surplus for a fully irrigated landscape, computed monthly, $\text{NDVI}_{nonirr}(t)$ = NDVI for the nonirrigated urban landscaping endmember, computed monthly.

Theoretically, if an urban pixel has a surplus of NDVI, meaning it has more NDVI than would occur naturally, it is hypothesized that the pixel is being supported by irrigation. Fig. 4 shows that NDVI_$S(t)$ has a seasonal pattern, with larger values during the summer months and smaller values during the winter months. Actual water-delivery to the 65 neighborhoods shows a similar seasonal pattern as NDVI_$S(t)$ (Fig. 4): water delivery was largest in the summer and smallest in the winter.

In order to establish a relationship between the NDVI_$S(t)$ and irrigation rates, one must start by scaling NDVI_$S(t)$ by the proportion of a neighborhood that is irrigated, incorporating $\overline{F_{irr}}$:

$$\text{NDVI\_}S_{nhood}(t) = \text{NDVI\_}S(t) * \overline{F_{irr}} \quad (6)$$

where $\text{NDVI\_}S_{nhood}(t)$ = the NDVI surplus of the composite neighborhood [recall that a neighborhood consists of irrigated and impervious fractions], computed monthly.

Next, water delivered to the neighborhood [$WD_{nhood}(t)$] must be separated into its two components: water used for landscape irrigation [$Irr_{nhood}(t)$] and the water used for other purposes, mostly household water use (HWU_{nhood}). HWU_{nhood} is assumed to be a constant.

$$WD_{nhood}(t) = HWU_{nhood} + Irr_{nhood}(t) \quad (7)$$

where $WD_{nhood}(t)$ = rate of water delivery to the composite neighborhood, computed monthly (mm/mo), HWU_{nhood} = water used by the composite neighborhood for purposes other than irrigation, constant (mm/mo), $Irr_{nhood}(t)$ = water used to irrigate the landscaping for the composite neighborhood, computed monthly (mm/mo).

Examination of the data from the San Fernando Valley suggests that $Irr_{nhood}(t)$ varies with time and is an exponential function of the NDVI surplus (Fig. 5). We can represent this relationship using a standard exponential equation:

$$Irr_{nhood(t)} = ae^{b*\text{NDVI\_}S_{nhood}(t)} \quad (8)$$

Substituting Eq. (8) into Eq. (7):

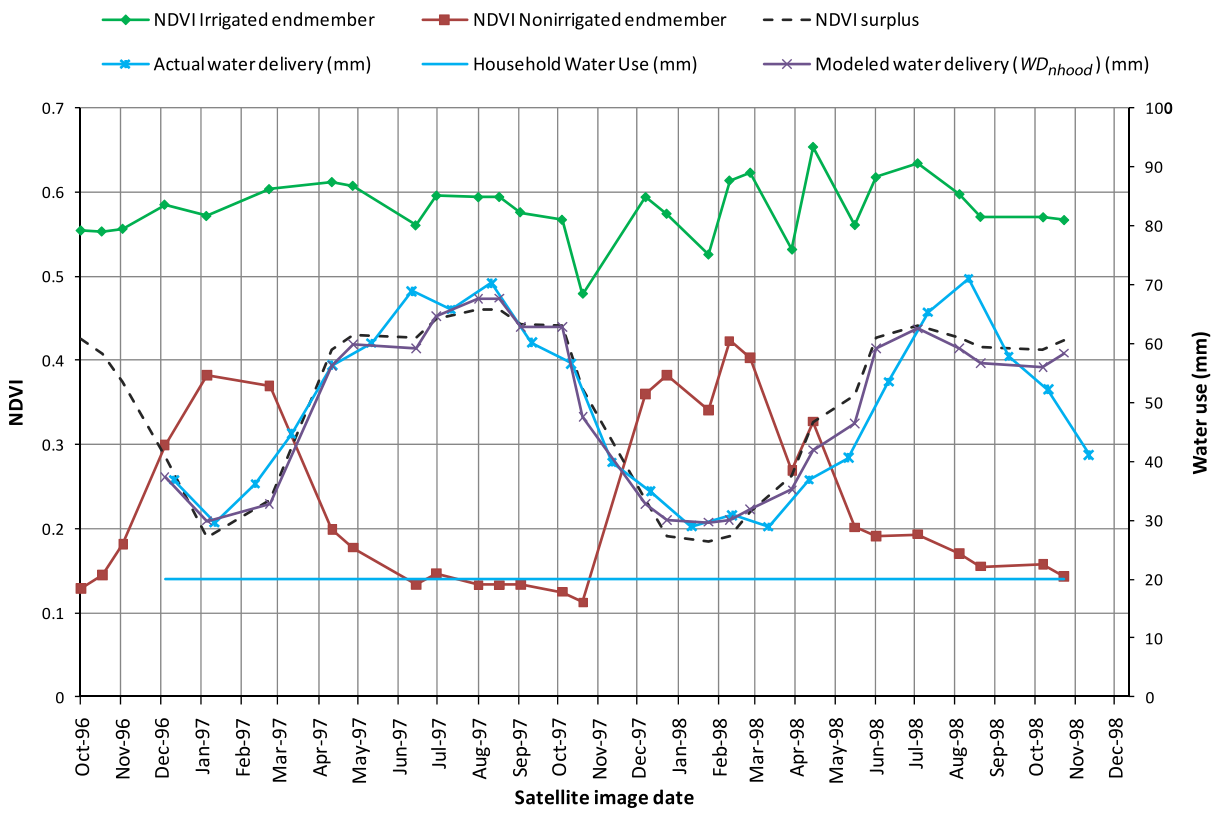

Fig. 4. Time-series plot of the NDVI surplus; NDVI for irrigated and nonirrigated endmembers shown for reference. Actual water delivery to the composite neighborhood, modeled water delivery, and household water use (shown as a constant line) are plotted on the secondary axis.

$$WD_{nhood}(t) = HWU_{nhood} + ae^{b*\mathrm{NDVI\_}S_{nhood}(t)} \quad (9)$$

In Eq. (9), HWU_{nhood} and the parameters a and b are unknowns. These unknowns were obtained by regressing $WD_{nhood}(t)$ and $\mathrm{NDVI\_}S_{nhood}(t)$ using the 20 months of data where a satellite image and water delivery data coincided for the 65 neighborhoods in the San Fernando Valley ($r^2 = 0.94$):

$$WD_{nhood}(t) = 20 + 3.3169e^{13.099*\mathrm{NDVI\_}S_{nhood}(t)} \quad (10a)$$

The second term in Eq. (10a) is the amount of water used for irrigation in the composite neighborhood (Eq. (8)), therefore, by removing the first term ($HWU_{nhood} = 20$) Eq. (10a) provides a basis for estimating urban irrigation rates from observed $\mathrm{NDVI\_}S_{nhood}(t)$ (Fig. 5):

$$Irr_{nhood(t)} = 3.3169e^{13.099*\mathrm{NDVI\_}S_{nhood}(t)} \quad (10b)$$

3.2.2. Using Landscape ET as surrogate for water-delivery records

Because water-delivery records are difficult to obtain, it would be useful to identify a surrogate for these records using data that are more readily available. Studies have shown that irrigation rates correlate with ET rates (Mayer et al., 1999; Keith et al., 2002). $ET_o(t)$ can be obtained from local meteorological stations such as CIMIS, or by using ET estimating functions such as SEBAL, METRIC or the Potential Evapotranspiration subroutine (POTEVAP) within the INFIL 3.0 software program (USGS, 2008). Therefore, establishing a correlation between ET and irrigation rates would be beneficial.

Once an appropriate reference ET is acquired, it must be scaled to estimate the landscape evapotranspiration rate [$ET_L(t)$]. $ET_L(t)$ was calculated using the following equation from CDWR (2000) with the addition of time (t):

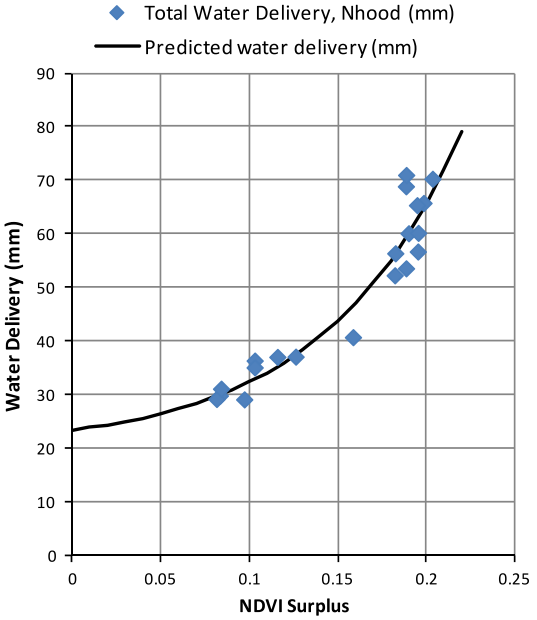

Fig. 5. Relationship between the total water delivered to the composite neighborhood and the NDVI Surplus. Points represent 20 months of data where water delivery and satellite data overlap. Irrigation for the neighborhood (Irr_{nhood}) can be substituted in the y-axis be subtracting 20 mm.

$$ET_L(t) = K_L * ET_o(t) \quad (11)$$

where $ET_L(t)$ = evapotranspiration for landscaped vegetation, computed monthly (mm/mo), K_L = landscape coefficient, constant, $ET_o(t)$ = reference potential evapotranspiration, computed monthly

(mm/mo). For the purposes of this study we used a K_L value of 0.65 (see Section 2.2).

Similar to NDVI_$S(t)$, $ET_o(t)$ is based on an area that is fully landscaped (i.e. no impervious land-cover). Direct comparison of $ET_L(t)$ and $Irr_{nhood}(t)$ requires an adjustment for the fraction of the area that is landscaped:

$$Irr_{wd}(t) = \frac{Irr_{nhood}(t)}{\overline{F_{irr}}} \tag{12}$$

where $Irr_{wd}(t)$ is the irrigation rate for a fully landscaped area, based upon NDVI surplus and calibrated using water-delivery records, computed monthly (mm/mo).

Time-series graphs of $Irr_{wd}(t)$ and ET_L (t) both show seasonal behavior, with a similar amplitude and wavelength; however, there is a slight phase shift between the two (Fig. 6). For example, from August through October when the ET_L (t) is dropping, irrigation amounts lag somewhat behind. Similarly, when ET_L (t) rises in March and April, irrigation again lags behind. This lag may be due to homeowners not immediately reacting to changes in ET, such as could occur when automatic sprinkler systems are adjusted only once or twice per year. Szilagyi et al. (1998) observed a similar 1-month lag between NDVI values and both evaporation and precipitation suggesting a phenological cause. It may be that residents adjust their irrigation rates based upon the greenness of their lawns, which may take a month to react to irrigation inputs.

Based upon the similarity between $Irr_{wd}(t)$ and $ET_L(t)$ shown in Fig. 6, a general estimate of urban irrigation could be calculated by multiplying the $ET_o(t)$ by 65% [as we did to compute $ET_L(t)$ in Eq. (11)]. Mayer et al. (1999) observed a similar relationship between outside water use and potential ET: 75% for both San Diego and Las Virgenes, CA. However, this method does not account for the lag we see in Fig. 6 nor does it allow for spatially applying an irrigation rate based upon the monthly NDVI signal. To account for both of these aspects, a scaling factor was computed using the available climate data and NDVI_$S(t)$ previously calculated in Eq. (5).

Computing a scaling factor converts the unitless values of NDVI_$S(t)$ into irrigation rates, and accounts for the lag effect shown in Fig. 6. Previously, the parameters for a and b in Eq. (9) were estimated using actual water delivery data. In the absence of these data, the coefficients a and b can be estimated from the observed NDVI and climatic data. The scaling factor was computed using an exponential function because the relationship between NDVI_S_{nhood} (t) and WD_{nhood} (t) was also exponential (Eq. (8)):

$$a = \frac{ET_{Lmax}}{e^{b*NDVI\_S_{max}}} \tag{13a}$$

$$b = \frac{\ln(ET_{Lmax}) - \ln(ET_{Lmin})}{NDVI\_S_{max} - NDVI\_S_{min}} \tag{13b}$$

where NDVI_S_{max} = characteristic high value for NDVI_$S(t)$, NDVI_S_{min} = characteristic low value for NDVI_$S(t)$, ET_{Lmax} = characteristic high value for $ET_L(t)$ (mm/mo), ET_{Lmin} = characteristic low value for $ET_L(t)$ (mm/mo).

Because Eqs. (13a) and (13b) use NDVI_S, Eq. (8) was rewritten so that it is applicable to all potentially irrigated pixels, instead of only the neighborhood. Therefore, the *nhood* subscript is dropped:

$$Irr(t) = ae^{b*NDVI\_S(t)} \tag{14}$$

where $Irr(t)$ is the irrigation rate for a fully landscaped area, based upon the NDVI surplus and $ET_L(t)$, computed monthly (mm/mo).

Maps of the location and rate of urban irrigation can now be created by multiplying $Irr(t)$ by $F_{irr}(t)$ on a pixel by pixel basis.

$$Irr_F(t) = Irr(t) \times F_{irr}(t) \tag{15}$$

where Irr_F is the irrigation amount based upon the fraction that a pixel is irrigated, computed monthly.

A flow chart documenting the sequence of steps for creating a distribution map of urban irrigation is shown in Fig. 7. The initial steps are to acquire the four datasets (ovals). Landsat imagery is then processed and NDVI calculated for each pixel. Using the air photos, target areas that represent the three endmembers are identified and their areas buffered inward by 15 m. The average NDVI value is then computed for these delineated areas, thus providing an NDVI value for each endmember. F_{irr} and NDVI_S are then calculated for each pixel. ET_L is a single value and is calculated from the climatic dataset; it is used in calculating Irr which is also a single value. Given Irr, Irr_F is then calculated for each pixel based upon F_{irr}. The last step involves clipping the results to only those areas that have the potential for irrigation based upon the land use dataset. This step could occur earlier if desired. The steps within the flow chart are for processing one image/month, and would be repeated

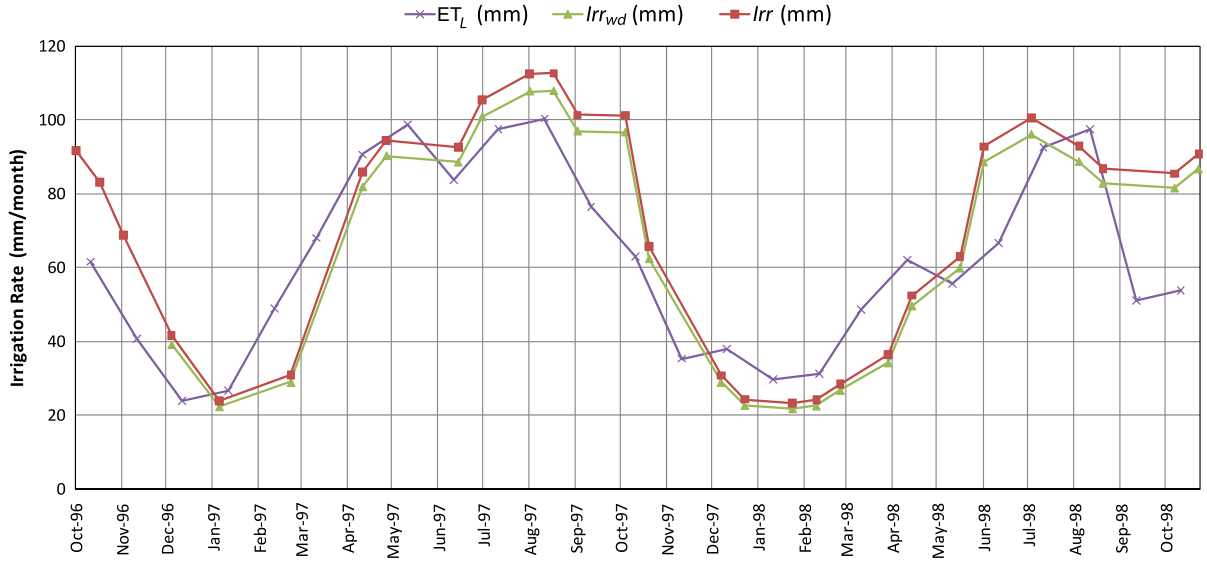

Fig. 6. Time-series plot of irrigation rates based upon (1) landscape evapotranspiration (ET_L) derived from the Glendale, CA CIMIS station, (2) the NDVI surplus, calibrated using water delivery records (Irr_{wd}), and (3) the NDVI surplus, calibrated using ET_L and scaling functions (Irr). All methods assume a fully irrigated and vegetated parcel of land.

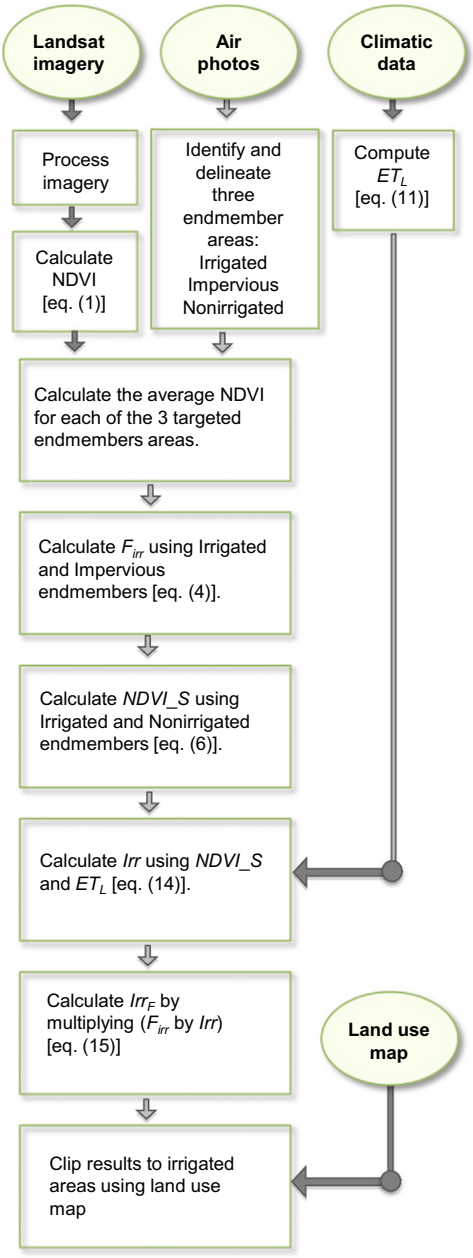

Fig. 7. Flow chart of the steps used for creating a distribution map of urban irrigation. Where: F_{irr}, = fraction of irrigated landscaping; NDVI_*S* = NDVI surplus; ET_L = Evapotranspiration for landscaped vegetation; *Irr* = Irrigation rate for a fully landscaped pixel; Irr_F = Irrigation rate for a pixel based upon the amount of irrigated landscaping it contains.

for each additional image/month (with the exception of delineating the endmembers which is only performed once).

4. Results

This section presents the results of both the validation of the methodology and the application of the methodology to the San Fernando Valley.

The first goal was to determine if NDVI endmembers can be used to estimate the amount of irrigated landscaping. However, to validate the model, the two-endmember model must first be shown to successfully predict NDVI values. We justified the use of a two-endmember mixture model by comparing the results with a more complicated three-endmember mixture model. A three-endmember mixture model was used because it is based upon the three land-cover components of a typical neighborhood: irrigated landscaping, impervious hardscape, and water body. A successful result would justify the use of an endmember model and affirm the selection of our endmembers.

$$\mathrm{NDVI}_{3end}(t) = (F_{irr} * \mathrm{NDVI}_{irr}(t)) + (F_{impv} * \mathrm{NDVI}_{impv}(t)) + (F_w * \mathrm{NDVI}_w(t)) \quad (16)$$

where $\mathrm{NDVI}_{3end}(t)$ = NDVI value for a single-family residential neighborhood, computed monthly, F_w = fraction classified as water body, $\mathrm{NDVI}_w(t)$ = NDVI for the water-body endmember, computed monthly.

The results from hand digitizing 13 randomly selected residential neighborhoods show that they consist of 57% impervious, 42% irrigated landscaping, and 1% water body. The observed NDVI values for these same endmembers were plotted on a time-series chart (Fig. 3). The percentages and observed NDVI values for the endmembers were inputted into a three-endmember Eq. (16) to calculate $\mathrm{NDVI}_{3end}(t)$ for the neighborhoods (Fig. 3). The computed values of $\mathrm{NDVI}_{3end}(t)$ compare favorably with the observed values of NDVI for the 65 neighborhoods at the 0.95 confidence level ($p = 0.0014$) using a paired *t*-test. Therefore, the three-endmember linear-mixture model was successful at modeling the observed neighborhood NDVI (Fig. 3).

The difference between $\mathrm{NDVI}_{2end}(t)$ and $\mathrm{NDVI}_{3end}(t)$ for any given month was less than 2%. Comparing the two methods statistically reveals no difference at the 0.95 confidence level ($p < 0.0001$). Therefore, the two-endmember model was selected for modeling the observed neighborhood NDVI because the water body endmember composed only 1% of the composite neighborhood. In addition, it has been shown that a minimum number of endmembers is ideal to reduce errors (Sabol et al., 1992).

These results justified the rearrangement of Eq. (2) into Eq. (3) so that the fraction of irrigated landscaping can be calculated from observed NDVI values. We used Eq. (4) to calculate $\overline{F_{irr}}$ as a check. The computed $\overline{F_{irr}}$ was 44.3%, and the hand-digitized fraction was 42.1%. This close correspondence indicates that a two-endmember binary mixture model, is a good approximation of the hand-mapped calculation of irrigated landscaping.

Fig. 3 shows the calculated $\mathrm{NDVI}_{2end}(t)$ and the observed NDVI values for the 65 neighborhoods on a time-series plot for comparison. These results indicate that the location and fraction of irrigated landscaping can be successfully estimated using satellite imagery by inputting the observed NDVI values for a targeted area and the observed NDVI values of two endmembers into a binary mixture model.

The second goal was to determine if irrigation rates could be estimated using ET as a surrogate for water delivery data. However, we needed to first separate the water delivery into its two components: irrigation [$Irr_{nhood}(t)$] and other household water uses (HWU_{nhood}), and to determine if our estimates were accurate. The volume of water used for purposes other than irrigation by a typical household in the San Fernando Valley was computed from the regressed value of *HWU* (20 mm) and the average lot size in the 65 neighborhoods [887 m^2; computed from the average neighborhood size (24,828 m^2) and the average number of homes (28)]. The resulting value of 583 l/day is within the range of the published values for indoor water use from the Mayer et al. (1999) study that showed 589 l per day for households in San Diego, CA, 771 l per day for households in Las Virgenes, CA. Although an irrigation value of 3.3169 mm/mo is theoretically possible when $\mathrm{NDVI\_}S_{nhood} = 0$, $\mathrm{NDVI\_}S_{nhood} = 0$ was not observed in the neighborhoods (Fig. 4).

Based upon Fig. 4, nearly 1/3 of the total water delivery during the winter months was used for irrigation. This indicates that single-family neighborhoods do not cease watering during the

wettest months; this result supports other research suggesting that the minimum-month method underestimates water use (CDWR, 1994; DeOreo et al., 1996; Mayer et al., 1999; Gleick et al., 2003). During the summer, outside water use expands to two-thirds of the total water use, also based upon Fig. 4. This result agrees with the results from the Mayer et al. (1999) study where 63% of water deliveries were used outside the home in August in San Diego, CA, and 82% in Las Virgenes, CA.

These results, in addition to the strong exponential correlation between $WD_{nhood}(t)$ and NDVI_$S_{nhood}(t)$ ($r^2 = 0.94$) justified a comparison of the predicted and actual irrigation rates for a fully irrigated parcel. Fig. 6 shows they both have a similar seasonal pattern. Actual irrigation was calculated by subtracting the household water-use constant (HWU_{nhood}) from the total water delivery data for the composite neighborhood and scaling the result up to a 100% landscaped area. Predicted water use was estimated using Eqs. (4), (5), (6), (13a), (13b), (14). There was no statistical difference between the two methods – one using water delivery data and one using climatic data – using the paired Wilcoxan signed-rank test ($p = 0.0063$). Therefore, the monthly irrigation rate for a fully irrigated parcel can be calculated using NDVI_S, climatic data, and scaling functions.

Finally, a pixel based map can be generated using Eq. (15). The results were constrained to those urban land-use classes that have the potential to be irrigated (Table 1).Fig. 8 shows maps of January and August 1997 irrigation rates calculated using Eq. (15) to illustrate the seasonality of urban irrigation. The street and road networks are clearly identifiable in both the January and August maps as light blue/gray colors where less/no irrigation occurred. Golf courses and parks are also identifiable by the darker blue colors, indicating more irrigation occurred. In general, the January map appears less blue than the August map because less irrigation occurred in January than in August. The maximum irrigation amount for January 1997 within the San Fernando Valley study area was 34.2 mm with an average of 9.5 mm (negative values were reclassified to zero). The maximum amount of irrigation for August 1997 was 152.5 mm with an average rate of 45.1 mm.

5. Discussion

The methodology presented in this paper was developed using single-family residential neighborhoods. The applicability of the methodology to other land-use classes was tested. Two tests were implemented: (1) the fraction of irrigated landscaping within other land-use classes was hand-mapped and compared to $\overline{F_{irr}}$, and (2) other data sources that map irrigated landscaping were compared with $\overline{F_{irr}}$. This section describes these efforts.

Three of the top five land-use classes within the San Fernando Valley were calculated for $\overline{F_{irr}}$ and compared with the hand-mapped calculations: (1) high-density single-family residential, (2) low-rise apartments, condos, and townhomes, and (3) strip malls. Two of the five land-use classes did not contain irrigated landscaping, therefore $\overline{F_{irr}}$ was not calculated, nor were they hand-mapped. (See Section 2.3 for further description.) $\overline{F_{irr}}$ for the high-density single-family residential land-use class was 44.2% whereas the hand-mapped value was 42.3%, a difference of 1.9% (the equivalent of less than 5% error). $\overline{F_{irr}}$ was markedly higher for the other two land-use classes (Table 2, Fig. 9). One possible cause of the overestimation could be that these areas have more trees and bushes relative to grass than single-family residential areas, consequently more canopy cover as seen from the satellite. Whereas, only the footprint of the vegetation was hand-mapped. These two land-use classes comprise about 9% of the total area therefore; the overestimate of irrigation is relatively small.

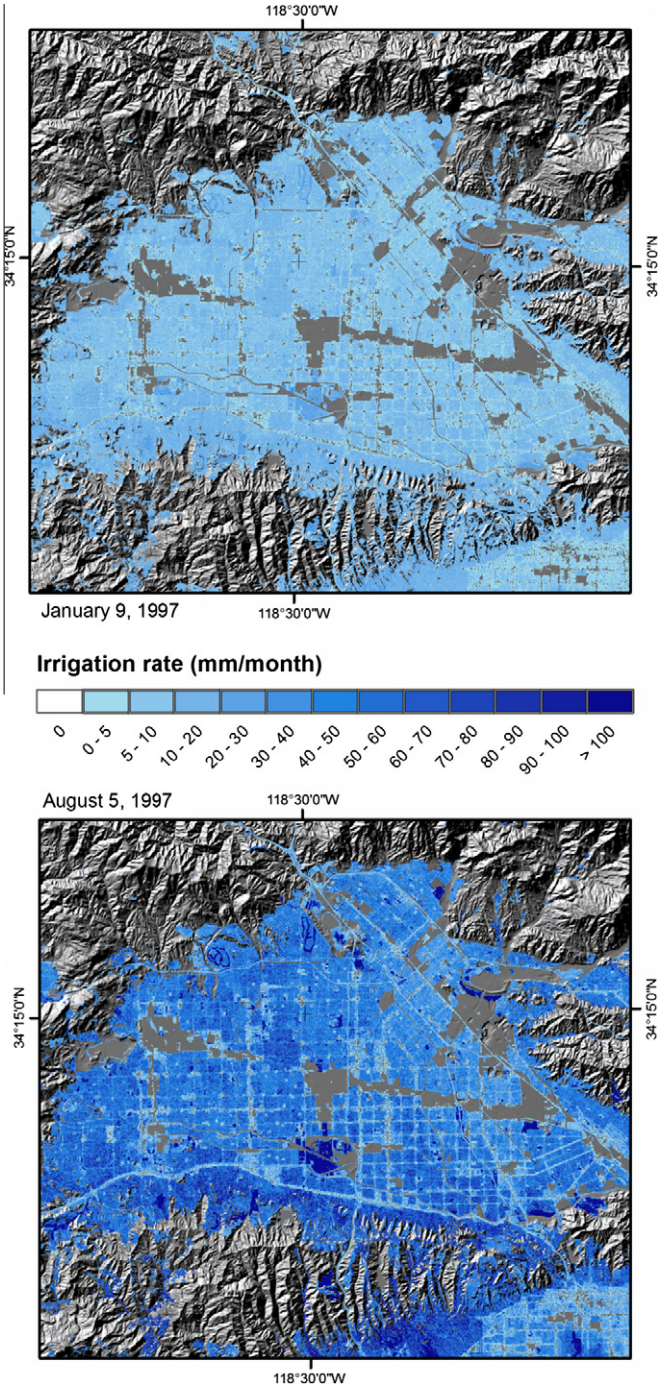

Fig. 8. The location and rate of urban irrigation within the vicinity of the San Fernando Valley for two satellite dates. (January 9, 1997 and August 5, 1997).

Additional work would be needed to validate and adjust for differences in landscaping practices among land-uses.

Two other independent datasets were examined to determine if their reported estimates of percent impervious can be compared with the hand-digitized and computed values of $\overline{F_{irr}}$. The datasets were the National Land Cover Dataset (NLCD) from the USGS (2003) and the Los Angeles County Department of Public Works (LACDPW, 2006). These datasets did not actually measure the amount of irrigated landscaping, instead they measured percent impervious. By assuming the inverse of the percent impervious is the percent pervious, and also assuming that pervious areas in an urban environment are being irrigated, we can compare percent

Table 2
Three land-use classes were compared using four methods for estimating the percentage of irrigated landscaping. The hand-digitized method was considered the ground-truth.

Land use code	Class	Description	Number of areas digitized	Hand-digitized fraction irrigated	$\overline{F_{irr}}$	NLCD	LACDPW[a]
1111	Residential	High-density single family residential	13	42.1	44.2	52.7	58
1123	Residential	Low-rise apartments, condominiums, and townhouses	17	17.0	31.1	42.4	14
1223/1224	Commercial	Modern/older strip development	17	3.5	8.8	32.2	3.5

[a] Values are for entire land use class.

pervious with both our calculated and digitized measure of $\overline{F_{irr}}$ (See Section 2.3) The NLCD dataset was systematically high in estimating irrigated landscaping (Table 2). The LACDPW dataset mapped the lesser vegetated land-use classes well, but overestimated single-family residential areas (58% as compared to 42.1%). The satellite based $\overline{F_{irr}}$ better approximated the hand-mapped values for the single-family residential land-use class than either the NLCD or the LACDPW (Fig. 9, Table 2). This result is rather expected because assuming that all pervious areas are being irrigated may not be true. There may be vacant urban areas that are not irrigated and yet are pervious. Alternatively, $\overline{F_{irr}}$ is calculated using NDVI and should therefore more accurately identify vegetation that is growing.

The hand-digitized fraction of irrigated landscaping for the 13 randomly selected neighborhoods was considered the ground-truth due to the high resolution it was mapped at. However, the difference between $\overline{F_{irr}}$ and hand-mapping could be caused by the difference in image dates. The satellite images were dated in the late 1990s and the air photos were dated in the mid to late 2000s. Therefore, the landscaped area within the 13 hand-digitized neighborhoods could have decreased slightly, as could occur when a swimming pool or driveway is added, or when a room addition is built. In this case, the difference between $\overline{F_{irr}}$ and the hand-digitized fraction could be even smaller than the reported 1.9%; however, this difference was considered a good correspondence.

Ideally, air photos (used for delineating the endmembers) and the satellite imagery would be similar temporally. If a user were to delineate endmembers using air photos from a different time period than the satellite imagery, it would be advisable to verify that the endmember existed at the time of the satellite imagery. For example, if a golf course was used as the irrigated endmember, it would be necessary to verify that the golf course existed during the satellite image date. We accomplished this check by acquiring b/w air photos from NAPP dated 1994. These air photos were not used in delineating the endmembers or in hand-digitizing because they were of lower resolution (1 m). For our study, it was more important for the satellite image dates to correspond with the water-delivery data, (which were acquired in a previous study) to allow for calibration purposes.

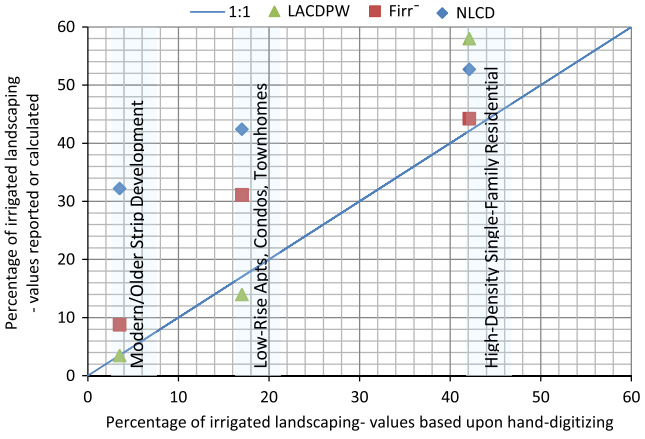

Fig. 9. Graph comparing the percentage of irrigated landscaping for three land-use classes using three different sources. Points above the 1:1 line have overestimated the amount of irrigated landscaping, points below have underestimated it, as compared to the hand-digitized method.

In regards to applying the methodology, it is important to apply Eq. (15) only to irrigated land-use classes because NDVI_$S(t)$ can be calculated for any vegetated area, whether irrigated or not. Natural vegetation, with a high NDVI_$S(t)$, would appear as if it were irrigated because the method is calibrated using nonirrigated urban landscaping. Nonirrigated urban landscaping will brown without supplemental irrigation in the summer whereas natural vegetation, such as riparian areas or the local chaparral in the surrounding hills, remain green throughout the year.

An additional consideration that should be made before applying the methodology is the validity of the land-use map. If a land-use class is designated as being irrigated, then all vegetated areas within that land-use class have the potential to receive irrigation. For example, a land-use map may identify an area as single-family residential, however, not every vegetated area within the residential neighborhood may actually be receiving irrigation. A more sophisticated method that could incorporate whether each pixel resembles a natural NDVI signal or an irrigated NDVI signal could be constructed in future research.

Other satellite imagery platforms could potentially be used with this methodology depending on the requirements for the project. Higher-resolution multispectral-imagery (10 m pixel size or less are available) could potentially delineate urban irrigated areas with greater precision; however, the scene size is often considerably smaller than Landsat requiring more scenes to cover the same area. In addition, higher resolution satellites usually have a cost-per-scene, whereas Landsat is free of charge. Also, many commercial satellites are "on-demand" and do not provide continuous coverage for a given area at high resolution. Because of this, the user should be careful in selecting the optimum satellite scenes to insure that the imagery is representing the extremes of the NDVI cycle. Moderate-Resolution Imaging Spectroradiometer (MODIS), has an NDVI product available with 16 day revisit frequency and up to 250 m resolution. The advantage of this product is that NDVI has already been calculated for the user. However, it is unclear if this resolution would be adequate to identify appropriate endmembers and to estimate irrigated landscaping using the binary mixture model. Future research could establish the viability of using MODIS or other imagery for this methodology.

The current analysis is based upon the 13 neighborhood scale, or approximately 1/3 km^2 square. At this resolution, the landscape was modeled into irrigated and nonirrigated components. If higher resolution imagery were to be used, additional components such as shadows or bare soil may need to be incorporated. Further investigation to identify smaller applicable scales could be useful for future analysis.

The methodology presented here is based upon a semi-arid Mediterranean climate of Southern California with a clearly identifiable hot/dry season and cool/wet season. Typical urban landscaping for this area consists of perennial grass, trees and bushes. This

type of vegetation, especially the grasses, will wilt and desiccate without additional irrigation inputs in the summer. Additional areas with differing climate, differing vegetation, and water-use patterns could be investigated to help make the methodology more robust and applicable in other areas. For example, and area with a predominance of trees could require the landscape coefficient (K_L) to be adjusted downwards.

6. Conclusions

The volume of water being applied to landscaped areas can exceed natural rainfall amounts in arid and semi-arid climates. This paper describes a new approach using readily available datasets for estimating the location and rate of urban irrigation. The approach has the added benefit of being able to map the spatial distribution and rate of irrigation historically as long as applicable input datasets are available.

The fraction of irrigated landscaping (F_{irr}) was modeled using two NDVI endmembers as inputs into a binary-mixture model. This method of identifying irrigated landscaping through remote sensing is beneficial because (a) it is not dependent on high resolution air photos which may not be historically available; (b) it is repeatable and consistent, and (c) can be calculated at the pixel level yet covering hundreds of square kilometers. As a test of the accuracy, $\overline{F_{irr}}$ was computed using the multi-scene average of F_{irr}. $\overline{F_{irr}}$ calculated in this way was 44%, similar to the hand-mapped method of 42%. This close correspondence indicates that a two-endmember binary mixture model, is a good approximation of irrigated urban landscaping.

The NDVI surplus [NDVI_$S(t)$] and climatic data were used to estimate the irrigation rate for irrigated areas. The surplus is defined as the NDVI value over that which would occur from precipitation alone. NDVI_$S(t)$ was calculated by subtracting the NDVI value from the irrigated landscaping endmember from the NDVI value from the nonirrigated landscaping endmember, and using climatic data to convert the unitless NDVI_$S(t)$ values into irrigation amounts. This method of calculating irrigation is advantageous because it is not dependent on water-delivery data, which can be difficult to acquire, and like F_{irr}, can be calculated at the pixel level using readily available datasets. It is also repeatable and consistent. Comparison of modeled irrigation rates with actual irrigation rates (based on water-delivery data from single-family residential neighborhoods) showed no statistical difference between the two (paired Wilcoxan signed-rank test, $p = 0.0063$). Therefore, the monthly irrigation rate for a fully irrigated parcel can be calculated using NDVI_S, climatic data, and scaling functions.

Maps of the location and rate of irrigation can be created by multiplying the fraction of irrigated landscaping $F_{irr}(t)$ by the irrigation rate $Irr(t)$ on a pixel-by-pixel basis. This method can be used for any given satellite scene. Maps representing January and August were created for the San Fernando Valley to illustrate the difference in applied water between winter and summer.

Acknowledgments

This work was funded by the USGS Groundwater Resources Program. We thank our colleagues at the USGS, including Eric Reichard, Peter Martin, Tracy Nishikawa, and La Rue Smith for their suggestions and comments, and Whitney Seymour for her technical support. We also thank the anonymous reviewers for their helpful comments.

References

Adams, J.B., Sabol, D.E., Kapos, V., Filho, R.A., Roberts, D.A., Smith, M.O., Gillespie, A.R., 1995. Classification of multispectral images based on fractions of endmembers: application to land-cover change in the Brazilian Amazon. Remote Sens. Environ. 52, 137–154.

Alcamo, J.M., Vörösmarty, C.J., Naiman, R.J., Lettenmaier, D.P., Pahl-Wostl, C., 2008. A grand challenge for freshwater research: understanding the global water system. Environ. Res. Lett. 3.

Allen, R.G., Tasumi, M., Morse, A., Trezza, R., 2005. A landsat-based energy balance and evapotranspiration model in Western US water rights regulation and planning. Irrig. Drain. Syst. 19, 251–268.

Allen, R.G., Tasumi, M., Morse, A., Trezza, R., Wright, J.L., Bastiaanssen, W., Kramber, W., Lorite, I., Robison, C.W., 2007. Satellite-based energy balance for mapping evapotranspiration with internalized calibration (METRIC) – applications. J. Irrig. Drain. Eng. 133 (4), 395–406.

Bastiaanssen, W.G.M., Menenti, M., Feddes, R.A., Holtslag, A.A.M., 1998. A remote sensing surface energy balance algorithm for land (SEBAL) 1. Formulation. J. Hydrol. 212–213, 198–212.

Bastiaanssen, W.G.M., Noordman, E.J.M., Pelgrum, H., Davids, G., Thoreson, B.P., Allen, R.G., 2005. SEBAL model with remotely sensed data to improve water-resources management under actual field conditions. J. Irrig. Drain. Eng. 131 (1), 85–93.

California Department of Water Resources, 1975. California's ground water. State of California Bulletin No. 118, 8 p.

California Department of Water Resources, 1994. Urban water use in California. State of California Bulletin No. 166-4.

California Department of Water Resources, University of California Cooperative Extension, 2000. A guide to estimating irrigation water needs of landscape plantings in California: The landscape coefficient method and WUCOLS III, pp. 1–150.

California Department of Water Resources, 2010. California Irrigation Management Information System (CIMIS), Reference Evapotranspiration Zones, 4 p.

Chander, G., Markham, B.L., Helder, D.L., 2009. Summary of current radiometric calibration coefficients for Landsat MSS, TM, ETM+, and EO-1 ALI sensors. Remote Sens. Environ. 113, 893–903.

Chen, J.M., Cihlar, J., 1996. Retrieving leaf area index of boreal conifer forests using Landsat TM images. Remote Sens. Environ. 55, 153–162.

City of Los Angeles Department of Water and Power, 2000. 1999–2000 Annual report. City of Los Angeles, Los Angeles, CA.

City of Los Angeles Department of Water and Power, 2001. Urban water management plan: fiscal year 2000–2001 annual update. City of Los Angeles, Los Angeles, CA.

Courault, D., Seguin, B., Olioso, A., 2005. Review on estimation of evapotranspiration from remote sensing data: from empirical to numerical modeling approaches. Irrig. Drain. Syst. 19, 223–249.

DeOreo, W.B., Heaney, J.P., Mayer, P.W., 1996. Flow trace analysis to assess water use. J. Am. Water Works Assoc. (January).

Gleick, P.H., Haasz, D., Henges-Jeck, C., Srinivasan, V., Cushing, K.K., Mann, A., 2003. Waste Not, Want Not: The Potential for Urban Water Conservation in California. Pacific Institute for Studies in Development, Environment and Security, 165p.

Grimmond, C.S.B., Oke, T.R., 1986. Urban water balance, 2. Results from a suburb of Vancouver, British Columbia. Water Res. Res. 22 (10), 1404–1412.

Grimmond, C.S.B., Oke, T.R., Steyn, D.G., 1986. Urban water balance, 1. A model for daily totals. Water Res. Res. 22 (10), 1397–1403.

Groeneveld, D.P., Baugh, W.M., Sanderson, J.S., Cooper, D.J., 2007. Annual groundwater evapotranspiration mapped from single satellite scenes. J. Hydrol. 344, 146–156.

Homer, C., Huang, C., Yang, L., Wylie, B., Coan, M., 2004. Development of a 2001 national land-cover database for the United States. Photogramm. Eng. Remote Sens. 70 (7), 829–840.

Hurd, B., Leary, N., Jones, R., Smith, J., 1999. Relative regional vulnerability of water resources to climate change. J. Am. Water Resour. Assoc.: Am. Water Resour. Assoc. 35 (6), 1399–1409.

Jacobs, K., Adams, D.B., Gleick, P., 2001. Potential consequences of climate variability and change for the water resources of the United States. In: National Assessment Synthesis Team (Ed.), Climate Change Impacts on the United States: The Potential Consequences of Climate Variability and Change. Report for the US Global Change Research Program. Cambridge University Press, United Kingdom, p. 620p.

Jensen, J.R., 2000. Remote Sensing of the Environment: An Earth Resource Perspective. Prentice Hall, New Jersey, 544 pp.

Johnson, T.D., 2005. Predicting residential irrigation amounts using satellite remote sensing in Los Angeles, California. Master's thesis, San Diego State University, 73p.

Keith, D.J., Walker, H.A., Paul, J.F., 2002. Terrestrial vegetation greenness of the lower Galveston Bay watershed from satellite remote sensing and its relation to water use and the salinity regime of the Galveston Bay Estuary (USA). Int. J. Remote Sens. 23 (5), 905–916.

Lu, D., Weng, Q., 2004. Spectral mixture analysis of the urban landscape in Indianapolis with Landsat ETM+ imagery. Photogramm. Eng. Remote Sens. 70 (9), 1053–1062.

Los Angeles County Department of Public Works, Water Resources Division, 2006. Hydrology manual. Appendix D, Proportion Impervious Data. Digital polygon dataset.

Ma, Z., Hart, M.M., Redmond, R.L., 2001. Mapping vegetation across large geographic areas: integration of remote sensing and GIS to classify multisource data. Photogramm. Eng. Remote Sens. 67 (3), 295–307.

Mayer, P.W., DeOreo, W.B., Opitz, E.M., Kiefer, J.C., Davis, W.Y., Dziegielewski, B., Nelson, J.O., 1999. Residential End Uses of Water. American Water Works Association Research Foundation, Denver, CO. 109 p.

Milesi, C., Running, S.W., Elvidge, C.D., Dietz, J.B., Tuttle, B.T., Nemani, R.R., 2005. Mapping and modeling the biogeochemical cycling of turf grasses in the United States. Environ. Manage. 36 (3), 426–438.

Myneni, R.B., Hall, F.G., Sellers, P.J., Marshak, A.L., 1995. The interpretation of spectral vegetation indexes. IEEE Trans. Geosci. Remote Sens. 33 (2), 481–486.

National Oceanic Atmospheric Administration, 2002. Climatography of the United States No. 81, Monthly Station Normals of Temperature, Precipitation, and Heating and Cooling Degree Days 1971–2000, California. National Environmental Satellite, Data, and Information Service. National Climatic Data Center, Asheville, NC.

Qi, J., Marsett, R.C., Moran, M.S., Goodrich, D.C., Heilman, P., Kerr, Y.H., Dedieu, G., Chenbouni, A., Zhang, X.X., 2000. Spatial and temporal dynamics of vegetation in San Pedro River basin area. Sci. Dir. – Agri. Forest Meteorol. 105 (1–3), 55–68.

Ridd, M.K., 1995. Exploring a V–I–S (vegetation–impervious surface–soil) model for urban ecosystem analysis through remote sensing: comparative anatomy for cities. Int. J. Remote Sens. 16 (12), 2165–2185.

Roberts, D.R., Batista, G.T., Pereira, J.L.G., Waller, E.K., Nelson, B.W., 1998. Change identification using multitemporal spectral mixture analysis: applications in Eastern Amazonia. In: Ross, S.L., Elvidge, C.D. (Eds.), Remote Sensing Change Detection: Environmental Monitoring Methods and Applications. Ann Arbor Press, Ann Arbor, MI, pp. 137–161.

Rouse, J.W., Hass, R.H., Schell, J.A., Deering, D.W., 1974. Monitoring vegetation systems in the Great Plains with ERTS. In: Proceedings of the Third Earth Resources Technology Satellite-1 Symposium, Greenbelt. NASA SP-351, 3010-317.

Sabol Jr., D.E., Adams, J.B., Smith, M.O., 1992. Quantitative subpixel spectral detection of targets in multispectral images. J. Geophys. Res. 97 (E2), 2659–2672.

Sample, D.J., Heaney, J.P., 2006. Integrated management of irrigation and urban storm-water infiltration. J. Water Resour. Plan. Manage. 362, 373.

San Diego County Water Authority, 2001. Annual report 2001. San Diego County Water Authority, San Diego, CA, 48 p.

Song, C., 2005. Spectral mixture analysis for subpixel vegetation fractions in the urban environment: how to incorporate endmember variability? Remote Sens. Environ. 95, 248–263.

Southern California Area Governments, 2005, Los Angeles County land use. Digital polygon dataset.

Szilagyi, J., Parlange, M.B., 1999. Defining watershed-scale evaporation using a normalized difference vegetation index. J. Am. Water Resour. Assoc. 85 (5), 1245–1255.

Szilagyi, J., Rundquist, D.C., Gosselin, D.C., 1998. NDVI relationship to monthly evaporation. Geophys. Res. Lett. 25 (10), 1753–1756.

US Geological Survey, 2003. National Land Cover Dataset 2001. Digital raster dataset. <http://seamless.usgs.gov> (accessed 29.06.10).

US Geological Survey, 2008. Documentation of computer program INFIL3.0 – A distributed-parameter watershed model to estimate net infiltration below the root zone: USGS Scientific Investigations Report 2008–5006. USGS, Reston, Virginia, 98 p..

US Census, 2008. American Community Survey (ACS) for the San Fernando Valley Sub-County Census District. (accessed 0.04.11).

Vörösmarty, C.J., Green, P., Salisbury, J., Lammers, R.B., 2000. Global water resources: vulnerability from climate change and population growth. Science 289, 284–288.

Western Resource Advocates, 2003. Smart water: A comparison of urban water use efficiency across the Southwest. 178p.